CHEMISTRY OF MATERIALS

Article

pubs.acs.org/cm

Isoindigo-Containing Molecular Semiconductors: Effect of Backbone Extension on Molecular Organization and Organic Solar Cell Performance

Yi Ren,[†,‡] Anna K. Hailey,[†] Anna M. Hiszpanski,[†] and Yueh-Lin Loo*[,†,‡]

[†]Department of Chemical and Biological Engineering, Princeton University, Princeton, New Jersey 08544, United States

[‡]Princeton Center for Complex Materials, Princeton University, Princeton, New Jersey 08544, United States

Supporting Information

ABSTRACT: We have synthesized three new isoindigo-based small molecules by extending the conjugated length through the incorporation of octyl-thiophene units between the isoindigo core and benzothiophene terminal units. Both UV−vis and Grazing incidence X-ray diffraction experiments show that such extension of the π-conjugated backbone can induce H-aggregation, and enhance crystallinity and molecular ordering of these isoindigo-based small molecules in the solid state. Compared to two other isoindigo-based derivatives in the series, the derivative with two octyl-thiophene units, BT-T2-ID, is the most crystalline and ordered, and its molecular packing motif appears to be substantially different. Devices utilizing these new extended isoindigo-based small molecules as the electron donor exhibit higher performance than those utilizing nonextended BT-ID as the electron donor. Particularly, devices containing BT-T2-ID in an as-cast blend with $PC_{61}BM$ show power conversion efficiencies up to 3.4%, which is comparable to the best devices containing isoindigo-based molecular semiconductors and is a record among devices containing isoindigo-based small molecules that were processed in the absence of any additives.

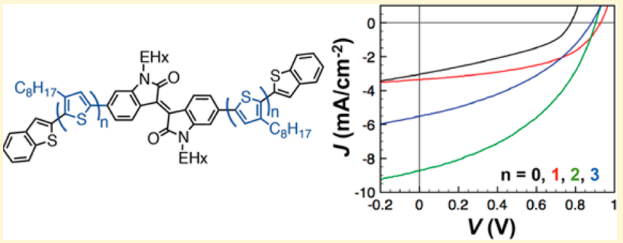

1. INTRODUCTION

In bulk heterojunction organic solar cells, the power conversion efficiency (PCE) depends not only on the individual chemical structures of the electron donor and acceptor materials, but also on the solid-state organization of the constituents.[1−6] While traditionally used as electron donor materials, π−conjugated polymers suffer from batch-to-batch variations in molecular weight and regioregularity that make controlling morphology, and ultimately device performance, difficult. Molecular semiconductors, on the other hand, can be purified more easily, and they do not suffer from molecular weight polydispersity;[1−3] their well-defined chemical and electronic structures provide a unique opportunity to systematically study the structure−function relationships that can guide the development of new high performance organic semiconductors.

Tuning the structure of molecular semiconductors can have a significant impact on their optical, structural, and electronic properties.[1−3] Extending the π−conjugated backbone of a molecular semiconductor, for example, is a popular route employed to generally increase the absorptivity and decrease optical bandgap of the parent compound so its absorption better matches the solar spectrum. Additionally, increasing the conjugation length can increase intermolecular π−π interactions, which can enhance molecular ordering and improve charge transport. However, the specific relationships between chemical structure and film structure remain complex and not well understood, in large part because they are not generalizable across families of compounds.

In the present investigation, we focus on the effect of backbone extension on the photophysical and structural properties of isoindigo-containing molecular semiconductors. The isoindigo moiety has been introduced as a strong electron-accepting unit for designing small bandgap donor−acceptor type molecular and polymeric semiconductors in organic solar cells.[7−12] Recently, the PCEs of polymer-based bulk-heterojunction solar cells comprising isoindigo-containing polymers have reached as high as 8%.[13] Compared to their polymeric counterparts, devices comprising isoindigo-based molecular semiconductors still lag behind in their PCEs.[14−18] Disappointingly, these new compounds have yielded devices that exhibit PCEs of ca. 2%[14−18] in the absence of any additives. Compared to other high-performing molecular electron donors, such as those containing 2,1,3-benzothiadiazole (BDT) and diketopyrrolopyrrole (DPP) moieties,[19−23] the solid-state structural characteristics of isoindigo-containing small molecules have not been fully addressed in the literature. Yet, systematic elucidation of the structure−property relationships of these compounds is needed to further explore and optimize their functionality as molecular semiconductors in organic solar cells.

Received: September 8, 2014
Revised: October 29, 2014
Published: October 29, 2014

   dx.doi.org/10.1021/cm503312c | Chem. Mater. 2014, 26, 6570−6577

On the basis of our previous studies of isoindigo-based small molecules, we found that electron-rich benzothiophene substitution at the 6,6′-positions of the isoindigo core results in a derivative that absorbs strongly in the visible and forms well-organized lamellar structures in the solid-state, characteristics that are correlated with higher performance when incorporated in organic solar cells compared to nominally similar derivatives having substitution at the 5,5′-positions.[24] As an extension from that work, we report herein the synthesis and characterization of second-generation isoindigo-based molecular semiconductors in which the conjugation length has been extended through the incorporation of octyl-thiophene moieties at the 6,6′-position, sandwiched between the isoindigo core and the benzothiophene terminal groups. The incorporation of multiple octyl-thiophene units is expected to further reduce the optical bandgap of these materials, effectively increasing its match with the solar radiation spectrum. Indeed, this reduction of bandgap has been shown with molecular isoindigo systems having thiophene extension in the absence of any solubilizing side chains and the benzothiophene terminal groups.[18] By incorporating octyl-thiophene units between the isoindigo core and benzithiophene terminal groups, we further show an enhancement of the molecular ordering. These materials perform more effectively as molecular electron donors in organic solar cells compared to the parent compound[24] or to derivatives having thiophene extension alone.[14−18]

2. EXPERIMENTAL SECTION

2.1. General. All manipulations were carried out under a dry nitrogen atmosphere employing standard Schlenk techniques. Commercially available chemicals were purchased from Sigma-Aldrich and Alfa Aesar, and were used as-received, unless otherwise noted. NMR solvents were purchased from Cambridge Isotope Laboratories. ^{1}H NMR and ^{13}C{1H}-NMR, were recorded on Bruker Avance (III) 300 and 500 MHz spectrometers. Chemical shifts were referenced to external TMS (^{13}C, ^{1}H). High-resolution mass spectra were obtained on a JEOL JMS-HX110A/110A tandem mass spectrometer. We sent our final products to Galbraith Laboratories, Inc., for elemental analyses. UV−vis experiments were carried out on a UV−vis-NIR Cary 5000 spectrophotometer. AFM was performed with a Veeco Dimension NanoMan microscope operated in tapping mode. Theoretical calculations were carried out at the B3LYP/6-31G(d) level using the GAUSSIAN 03 suite of programs.[25]

2.2. Device Fabrication. Patterned ITO (15 Ω/sq) on glass substrates was coated with 30 nm thick poly(3,4-ethylenedioxythiophene)/poly(styrenesulfonate), PEDOT/PSS (Clevios P), followed by thermal annealing at 150 °C for 10 min. The PEDOT/PSS was diluted with distilled water at 1:1 volume ratio prior to use. A 70−80 nm thick film of the donor and acceptor blend was obtained by spin-coating solutions of the new isoindigo derivatives and phenyl-C_{61}-butyric acid methyl ester ($PC_{61}BM$) at 1500 rpm for 30 s atop the PEDOT/PSS layer. The solution comprised of 1 mL of chloroform and 8 mg of donor; the mass of $PC_{61}BM$ was varied (8, 6, and 4 mg) during the optimization of the active layer. Lithium fluoride (1 nm) and aluminum (60 nm) top electrodes were thermally evaporated through a shadow mask at a pressure of 10^{-6} bar and an evaporation rate of 0.1 Å/s and 0.8 Å/s, respectively, to define an active area of 0.18 cm^2. Current density−voltage (J−V) characteristics were acquired using a Keithley 2635 source measurement unit under AM 1.5G 100 mW/cm^2 illumination in a nitrogen-filled glovebox (<0.1 ppm of O_2 and H_2O). Both hole and electron mobilities of the blends were extracted from space charge limited current (SCLC) measurements on hole- and electron-only devices, respectively. The hole-only devices use PEDOT/PSS and gold as electrodes, whereas the electron-only devices use aluminum as electrodes.

2.3. Grazing-Incidence X-ray Diffraction (GIXD) Experiments. GIXD experiments were conducted at the G1 and G2 stations of the Cornell High Energy Synchrotron Source. At the G1 station, the beam was selected to be 0.05 mm tall and 1 mm wide. The width of the samples was 0.5−0.7 cm; this smaller sample width was chosen to reduce geometric smearing of the peaks on the detector.[26] The beam energy was selected with synthetic multilayer optics (W/B4C, 23.6 Å d-spacing). Scattered intensity was collected with a two-dimensional CCD detector. At the G2 station, the beam was selected to be 0.2 mm vertical and 2 mm horizontal. The beam energy was selected using a beryllium single-crystal monochromator. Scattered intensity was collected using a 640-element 1D diode array. At both stations, the X-ray beam was aligned above the film's critical angle and below that of the substrate, at 0.16−0.17° with respect to the substrate. Variations in detector-to-sample distance were accounted for during data processing. Additionally, all GIXD images have been background subtracted, and polarization and absorption corrections were applied, though these corrections were generally small.[26]

3. RESULTS AND DISCUSSION

3.1. Synthesis. The synthetic steps that were carried out to access the isoindigo compounds are shown in Scheme 1. The

Scheme 1. Synthesis of Isoindigo Derivatives Having Extended Conjugated Cores[a]

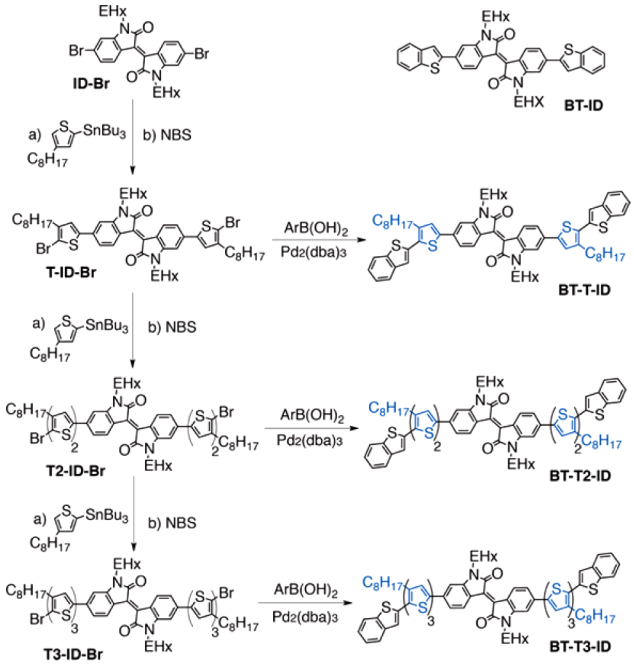

[a]BT-ID is the parent compound, referred to as m-BT in reference 24.

octyl-thiophene precursor, tributyl(4-octylthiophen-2-yl)-stannane, was synthesized according to previously reported procedures.[27] Stille coupling reaction and bromination were carried out to synthesize the dibromo precursors of T-ID-Br, T2-ID-Br, and T3-ID-Br. As a final step, these dibromo precursors were subjected to a Suzuki coupling reaction with benzothiophene-2-boronic acid, yielding the extended target compounds of BT-T-ID, BT-T2-ID, and BT-T3-ID. Additional synthetic details and characterization of these compounds are provided in Scheme S1 (Supporting Information). Differential scanning calorimetry (DSC) experiments conducted at a heating rate of 10 °C/min yielded melting temperatures of 249, 189, 134, and 139 °C, for BT-T-ID, BT-T2-ID, and BT-T3-ID, respectively (for scans, see Figure S10, Supporting

dx.doi.org/10.1021/cm503312c | Chem. Mater. 2014, 26, 6570−6577

Information). On heating, BT-T2-ID exhibits a cold crystallization transition at 78 °C that is not present during the heating of the other compounds.

3.2. Photophysical Properties. The UV−vis absorption of the isoindigo derivatives was measured in cyclohexane to minimize solvent polarity effects. These UV−vis spectra are provided in Figure 1a. We observe that the absorption spectra

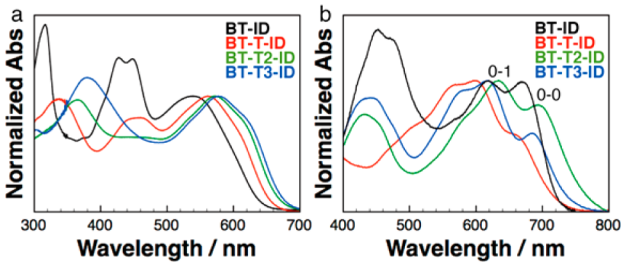

Figure 1. UV−vis absorption spectra of isoindigos (a) at concentrations $<10^{-5}$ mol/L in cyclohexane and (b) in annealed thin films. The spectra have been normalized at their respective low-energy λ_{max} for comparison.

of the isoindigo derivatives red-shift with increasing number of octyl-thiophene units due to an increase in the conjugation length. The absorption maximum, λ_{max}, increases from 538 nm for BT-ID (named m-BT in our previous study[24]) to 561 nm for BT-T-ID, to 571 nm for BT-T2-ID, and to 577 nm for BT-T3-ID. Given BT-T2-ID's limited solubility in cyclohexane, we have also conducted UV−vis characterization of the extended isoindigo compounds in chloroform (Figure S11a, Supporting Information) to estimate the molar extinction coefficients of these new isoindigo derivatives (tabulated in Table 1). As

Table 1. Photophysical Data of Isoindigo Derivatives

compound	λ_{max} (nm)[a]	ε[b]	E_{opt} (eV)[c]	HOMO (eV)[d]	LUMO (eV)[e]
BT-ID[f]	538 (553)	22 240	1.70	−5.44	−3.74
BT-T-ID	561 (585)	27 100	1.73	−5.33	−3.60
BT-T2-ID	571 (600)	86 000	1.60	−5.18	−3.58
BT-T3-ID	577 (606)	106 100	1.65	−5.12	−3.47

[a]Measured in cyclohexane; in parentheses, measured in chloroform. [b]Molar extinction coefficient ($L \cdot mol^{-1} \cdot cm^{-1}$) in chloroform. [c]Obtained from the onset of the lowest-energy absorption in thermally annealed thin films. [d]Determined by photoelectron spectrometer (AC-2) at atmospheric pressure on thermally annealed thin films. [e]$E_{LUMO} = \Delta E_{opt} - |E_{HOMO}|$ [f]Reported in ref 24.

expected, the molar extinction coefficients of the extended isoindigo derivatives are higher than that of BT-ID and increase with increasing number of octyl-thiophene units. Compared to the spectra acquired in cyclohexane, the spectra of isoindigo derivatives acquired in chloroform are red-shifted, but their vibronic features are substantially weakened. We attribute this observation to the presence of a more stabilized CT state in the more polar chloroform solutions.[28,29]

We also calculated the S_0-S_1 transition energy of the extended isoindigos by time-dependent (TD) density functional theory (DFT).[25,30] The frontier orbitals are shown in Figure S12 (Supporting Information) with the data summarized in Table S1 (Supporting Information). Consistent with experimental results, the calculated S_0-S_1 transition energy decreases with increasing number of octyl-thiophene units. In addition, the calculated oscillator strength also increases with increasing number of octyl-thiophene units, in line with the increasing molar extinction coefficients of their solutions.

Compared to the solution spectra, the solid-state spectra are more complicated. Generally, the spectra of the as-cast films (Figure S11b, Supporting Information) of the extended isoindigo derivatives are red-shifted relative to their solution spectra in cyclohexane. The red shift observed in the solid-state absorbance spectra can be attributed to increased intermolecular $\pi-\pi$ interactions in addition to enhanced planarity of the backbone in the solid state compared to in solution. Similar to our previous studies on BT-ID, thermal annealing at 100 °C for 5 h leads to a further red-shift in λ_{max} and the enhancement of vibronic structures in the solid-state absorption spectra of the extended isoindigos (Figure 1b). Unlike the solution spectra, however, the peaks in the solid-state absorption spectra do not shift to lower energy monotonically with the number of octyl-thiophene units. The solid-state absorption spectrum of BT-T-ID is, for example, blue-shifted compared to that of BT-ID, despite the fact that BT-T-ID has a longer conjugated backbone. Further increasing the number of octyl-thiophene units to two and three significantly red-shifts their solid-state absorption spectra, albeit to different extents. The spectrum of BT-T2-ID shows the most red-shift in its λ_{max} despite the fact that BT-T3-ID has the longest conjugated backbone. These observations are very different from those of isoindigo-containing oligothiophenes in the absence of any side chains and benzothiophene terminal groups, where the solid-state λ_{max} increases linearly with increasing number of thiophene units.[18] This difference implicates the role of the octyl side chains in driving molecular organization in the solid-state.

Compared to the solid-state spectrum of BT-ID, the solid-state UV−vis spectra of the extended isoindigo derivatives show 0−0 vibronic peak that is weaker than the 0−1 vibronic peak (Figure 1b). This observation also contrasts with those previously reported on isoindigo-containing oligothiophenes in the absence of any side chains where the intensity ratio between 0−0 and 0−1 vibronic peaks is higher than our compounds.[7,18] The experimental and theoretical studies of polythiophenes[31] suggest that this discrepancy in the intensity ratios of the vibronic peaks in the solid-state spectra stem from differences in the extent of planarization of the π-conjugated backbone as well as differences in $\pi-\pi$ stacking interactions in the solid state due to the presence of the octyl side chains. Based on these studies, we believe our extended isoindigo derivatives form H-aggregates in the solid state, different from the *J*-aggregates exhibited by the parent compound of BT-ID. The solid-state absorption spectrum of BT-T2-ID, in particular, shows a much stronger 0−0 vibronic peak compared to the absorption spectra of the other extended isoindigos at 733 nm, which also hints at differences in its solid-state organization compared to those of BT-T-ID and BT-T3-ID. This observation is similar to those of recently reported isoindigo polymers having oligothiophene spacers, in which the absorbance spectrum of a polymer having a bithiophene unit exhibits the strongest 0−0 vibronic peak compared to those of polymers having one and three thiophene units.[32]

The HOMO energy levels that were obtained on thin films of the isoindigo compounds increase monotonically upon increasing the number of octyl-thiophene units (Table 1). The optical bandgaps of the isoindigo derivatives were calculated from the onset of absorption of annealed films and are listed in Table 1. The solid-state optical bandgap does not decrease

dx.doi.org/10.1021/cm503312c | *Chem. Mater.* 2014, 26, 6570−6577

monotonically as observed in solution. BT-T2-ID exhibits the smallest bandgap of 1.60 eV; BT-T-ID shows the largest bandgap of 1.73 eV. BT-ID and BT-T3-ID display bandgaps of 1.70 and 1.65 eV, respectively.

3.2. Solid-State Structures. GIXD experiments were carried out to reveal the solid-state structure of these isoindigo derivatives. The GIXD patterns of the as-cast neat films are shown in Figure S13 (Supporting Information). In the GIXD pattern of BT-ID (Figure S3a, Supporting Information), we observe multiple reflections at q = 0.43, 0.63, 0.73, 0.83, 0.96, 1.05, and 1.14 Å^{-1}. These reflections give rise to q/q^* ratios of 1, $\sqrt{2}$, $\sqrt{3}$, $\sqrt{4}$, $\sqrt{5}$, $\sqrt{6}$, and $\sqrt{7}$, and suggest a body-centered cubic packing with a unit cell length of ca. 20.8 Å for as-cast BT-ID. The observation that the primary reflection is azimuthally anisotropic and is located on the meridian at q_z = 0.43 Å^{-1} indicates that the (110) plane is preferentially oriented out of the plane of the substrate. As for the GIXD patterns of the as-cast films of the extended isoindigo compounds, we observe two strong reflections along the meridian in their GIXD patterns (Figure S13b–d, Supporting Information). Given the limited number of reflections in the GIXD patterns, however, we are not able to identify the unit cell or any of the lattice parameters for these compounds. Still, we are able to extract some interesting structural observations. The fact that the second reflection occurs at twice the q-spacing as the first reflection in each case indicates that the reflections must arise from the same family of planes. Given the intensity anisotropy of these reflections, we can further ascertain that these planes are preferentially oriented out of the plane of the substrate, albeit to different extents as evidenced by differences in the azimuthal intensity distribution. Per the GIXD patterns shown in Figure S13 (Supporting Information), BT-ID and BT-T-ID as-cast thin films are less oriented than the as-cast thin films of BT-T2-ID and BT-T3-ID.

We further crystallized BT-ID, BT-T-ID, and BT-T3-ID by annealing these thin films at 100 °C for 5 h. The GIXD patterns of these annealed films are shown in Figure 2; they uniformly

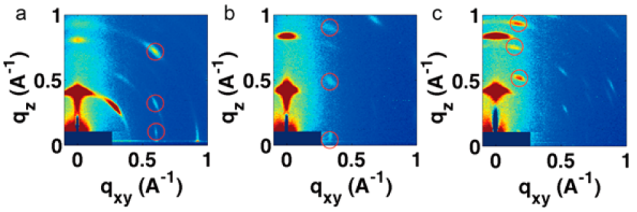

Figure 2. GIXD images of annealed films (100 °C for 5 h) of (a) BT-ID, (b) BT-T-ID, (c) BT-T3-ID.

display stronger and more numerous reflections compared to the GIXD patterns of their as-cast films. Analysis of the q/q^* ratios of the reflections in these GIXD patterns indicates that none of these molecules adopt a cubic unit cell in annealed thin films. The cubic phase that we access in as-spun BT-ID thin films thus appears to be a metastable polymorph. That molecular semiconductors exhibit different polymorphs based on processing routes is not unusual.[33] In each of the GIXD patterns presented in Figure 2, we observe two meridional reflections at q_z = 0.41 and 0.82 Å^{-1} that are suggestive of preferential out-of-plane orientation. Given the invariant placement of the meridional reflections, we surmise that BT-ID, BT-T-ID, and BT-T3-ID exhibit the same characteristic out-of-plane spacing of 15.3 Å on thermal annealing. It thus appears that the introduction of octyl side chain substituted thiophene moieties to the parent compound does not alter the out-of-plane spacing in these thermally annealed thin films. Interestingly, this out-of-plane d-spacing is also similar to that previously reported for isoindigo-containing oligothiophene without any side chain substitution and benzothiophene terminal groups (d = ca. 13.9–15.8 Å).[18]

On the other hand, that the 0–0 vibronic peaks in the solid-state absorbance spectra of our extended isoindigo derivatives are weaker compared to those in the absorbance spectra of isoindigo derivatives having oligothiophene substitutions without any side chain substitution and benzothiophene terminal groups[18] suggests that the presence of alkyl side chains does affect the intermolecular π–π interactions and the planarization of the π-conjugated backbone in the solid state. Given the two observations above, we are left to infer that intermolecular π–stacking must occur in a direction off the substrate normal. This circumspection is consistent with our previous analysis of the GIXD pattern of BT-ID.[24] When neat thin films of BT-ID are annealed at temperatures higher than that reported here, a sharp reflection in the diffraction pattern becomes visible at q = 1.7 Å^{-1} (3.7 Å); attributing this reflection to the characteristic π–π distance between adjacent molecules, we determined that the π–stacking direction of BT-ID is oriented 53° away from the substrate normal.[24]

In contrast with the invariant q_z spacing of the meridional reflections across the GIXD patterns in Figure 2, we observe differences in the q_{xy} spacing associated with the off-meridian reflections in the GIXD patterns of the annealed thin films. When all reflections in a GIXD pattern fall into a series of columns at constant values of q_{xy} (such as those highlighted in red circles in the GIXD patterns of BT-ID and BT-T-ID in Figure 2a,b), we can assume that the unit cell is oriented such that one of its axes is normal to the substrate. It follows that we can estimate the larger of the other two off-normal unit cell dimensions from the smallest q_{xy} position at which a column of such reflections are located. In the GIXD pattern of BT-ID (Figure 2a), for example, the column of reflections along q_{xy} = 0.6 Å^{-1} indicates that the larger off-normal unit cell dimension is 10 Å. We can ignore the two scattered reflections around q_{xy} = 0.3 Å^{-1}, because these reflections correspond to reflections from a secondary population of crystallites whose orientation is different from that of the primary population that has its parallel plane indicated by the more intense meridional reflection at q_z = 0.41 Å^{-1}. Using a similar reasoning, the larger off-normal unit cell dimension for BT-T-ID is 19 Å. It thus appears that the addition of one octyl-thiophene moiety increases this off-normal unit cell dimension by almost a factor of 2. We cannot, however, extend this analysis to the GIXD pattern of BT-T3-ID. Because we do not observe columns of reflections along specific q_{xy} (Figure 2c), the unit cell it adopts is not conveniently oriented with one of its axes normal to the substrate. In this situation, a higher-index plane must be parallel to the substrate, making extraction of the unit cell dimensions prohibitively difficult without more numerous reflections than are observed in Figure 2c.

The absorbance measurements and DSC experiments hint that BT-T2-ID is likely to adopt a structure that is substantially different from those of BT-ID, BT-T-ID, and BT-T3-ID. Indeed, BT-T2-ID is substantially more ordered; the GIXD pattern of its annealed thin film in Figure 3a exhibits many more reflections that are also more intense compared to those of the other compounds. Given the numerous reflections, we

dx.doi.org/10.1021/cm503312c | Chem. Mater. 2014, 26, 6570–6577

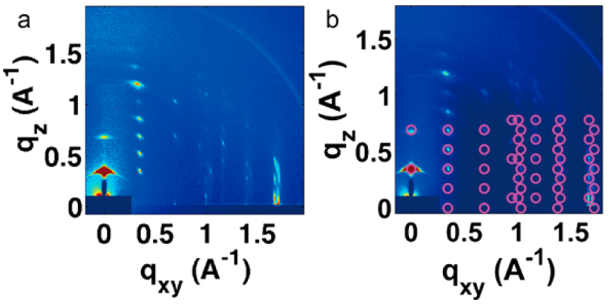

Figure 3. (a) GIXD image of an annealed film (100 °C for 5 h) of BT-T2-ID and (b) the same GIXD image with reflections calculated based on the *Pc* space group overlaid in magenta.

have been able to determine the lattice parameters and symmetry of a unit cell whose calculated X-ray diffraction pattern is consistent with that experimentally obtained on BT-T2-ID. The best fit with the DPC toolkit program[34] yields a monoclinic unit cell oriented with its (001) plane parallel to the substrate, having dimensions a = 6.6261 Å; b = 18.2574 Å; c = 36.3520 Å; and angles $\alpha = 90°$; $\beta = 95.4°$; $\gamma = 90°$. Taking into account the intensity anisotropy in the azimuthal direction, the c axis must be preferentially oriented out-of-plane. The largest off-normal dimension of BT-T2-ID is thus the b axis, with a spacing that is comparable to that of BT-T-ID.

We note, however, one peculiarity with BT-T2-ID. Properly accounting for all the experimental reflections during the fitting exercise mandates the meridional reflections at q_z = 0.34 Å^{-1} and 0.68 Å^{-1} to be the second- and forth-order reflections—instead of the first- and second-order reflections—in the out-of-plane direction. Indeed, close examination of the column of reflections at q_{xy} = 0.35 Å^{-1} confirms that the odd meridional reflections must be absent due to lattice symmetry. While our software does not specifically account for relative intensities of the reflections, which would have provided information about molecule placement within the lattice, we can account for lattice symmetries by considering different space groups. Given the systematic absence of the odd meridional reflections, we have narrowed the possible space groups to *Pc*, *P2/c*, or $P2_1/c$. The locations of the expected reflections if the unit cell belonged to the *Pc* space group and had the dimensions above are shown as magenta circles overlaying the X-ray diffraction pattern of BT-T2-ID in Figure 3b. We observe very good agreement between the calculated and experimental reflections. The calculated reflections for the *P2/c* and $P2_1/c$ space groups are provided in Figure S14 (Supporting Information) for completeness and for ease of comparison. They, too, yield comparably good fits to our experimental data. Returning to the meridional reflections, our analysis mandates the forbidden first-order, out-of-plane reflection to be at q_z = 0.17 Å^{-1}, corresponding to a characteristic d-spacing of 36.4 Å, which is much larger than the out-of-plane d-spacing of BT-ID, BT-T-ID, and BT-T3-ID, or those of any other isoindigo-containing molecular or polymeric semiconductor reported previously.[14,18,24,35−37] We note a similar peculiarity was reported for the isoindigo derivatives comprising oligothiophenes without any side chain substitution and benzothiophene groups, in which the two-thiophene derivative exhibits a larger d-spacing (d = ca. 19 Å) than the other derivatives (d = ca. 15 Å).[18]

Previously, it has been observed that the molecular organization of α-oligothiophenes can differ with the parity of the number of thiophene units, in which oligothiophenes having an even number of thiophene units adopt a well-defined crystal structure that is different from that adopted by oligothiophenes having an odd number of thiophene units.[38] Although our current study cannot confirm the presence of such an "even−odd effect,"[38] it is curious that the solid-state organization of BT-T2-ID is singularly different from those of BT-T-ID and BT-T3-ID. While we have thus far not been able to elucidate the specifics of the packing motifs because single-crystal growth attempts were not successful, differences in the solid-state organization between the isoindigo derivatives are mirrored in our absorption measurements, as discussed above. Such dramatic structural differences in the solid state should impart differences in device performance when BT-T2-ID, instead of the other compounds, is incorporated in solar cells.

3.3. Photovoltaic Properties and Morphological Characteristics of the As-cast Devices. The extended isoindigo-based small molecules were incorporated into bulk-heterojunction solar cells as electron donors with [6,6]-phenyl C61 butyric acid methyl ester ($PC_{61}BM$) as the electron acceptor. The performance of these devices is summarized in Table 2. As we previously reported, our optimized device

Table 2. Device Parameters of Optimized Solar Cells Containing Extended Isoindigo Derivatives and $PC_{61}BM$

donor	processing condition	V_{oc} (V)	J_{sc} (mA/cm^2)	FF (%)	PCE (%)[e]
BT-T-ID[a]	as-cast	0.84	4.9	42	1.7 (1.5 ± 0.2)
	annealed[d]	0.84	3.2	57	1.5 (1.4 ± 0.1)
BT-T2-ID[b]	as-cast	0.90	8.7	43	3.4 (3.2 ± 0.2)
	annealed[d]	0.83	5.3	50	2.2 (2.1 ± 0.1)
BT-T3-ID[c]	as-cast	0.91	6.0	40	2.2 (2.0 ± 0.2)
	annealed[d]	0.86	4.0	49	1.7 (1.6 ± 0.1)

[a]8 mg:6 mg. [b]8 mg:4 mg. [c]8 mg:6 mg. [d]After thermal annealing at 70 °C for 10 min. [e]Values in brackets are averages based on 4−5 devices.

having thermally annealed BT-ID and [6,6]-phenyl C71 butyric acid methyl ester ($PC_{71}BM$) shows a PCE of 0.87%.[24] However, devices containing the as-cast BT-ID and $PC_{71}BM$ blend only show a PCE of 0.01%.[24] Surprisingly, devices containing as-cast blends of BT-T-ID and $PC_{61}BM$ were optimized to give a maximum PCE of 1.7%, with a short-circuit current density (J_{sc}) of 4.9 mA/cm^2, an open-circuit voltage (V_{oc}) of 0.84 V, and a fill factor (FF) of 42%. The incorporation of extended isoindigo derivatives having additional octyl-thiophene moieties in solar cells leads to further improved performance, as shown in the $J-V$ characteristics in Figure 4a.

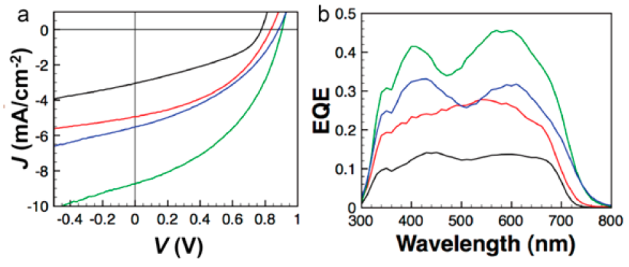

Figure 4. (a) $J-V$ characteristics and (b) EQE spectra of optimized bulk-heterojunction solar cells comprising (black) annealed BT-ID and $PC_{71}BM$, (red) as-cast BT-T-ID and $PC_{61}BM$, (green) as-cast BT-T2-ID and $PC_{61}BM$, (blue) and as-cast BT-T3-ID and $PC_{61}BM$.

dx.doi.org/10.1021/cm503312c | *Chem. Mater.* 2014, 26, 6570−6577

The best performing device, whose active layer comprises a blend of BT-T2-ID and $PC_{61}BM$ at a 2:1 mass ratio, exhibits a PCE of 3.4% with a J_{sc} of 8.7 mA/cm^2, a V_{oc} of 0.90 V, and a FF of 43%. To the best of our knowledge, this is the highest efficiency reported for devices comprising any isoindigo-based molecular semiconductors without the use of solvent additives.[11] Devices comprising BT-T3-ID and $PC_{61}BM$ exhibit a PCE of 2.2% with a J_{sc} of 6.0 mA/cm^2, a V_{oc} of 0.91 V, and FF of 40%. The corresponding external quantum efficiency (EQE) spectra for these devices are provided in Figure 4b. Consistent with the $J-V$ characteristics, the EQE spectrum of the device comprising BT-T2-ID and $PC_{61}BM$ shows the highest EQE between 300 and 800 nm.

The enhanced performance of devices comprising these extended isoindigo derivatives largely stems from an increase in the photocurrent compared to devices containing BT-ID. First, the extended isoindigo derivatives are more absorptive compared to BT-ID. Second, diodes containing extended isoindigo blends also show higher hole mobilities than diodes containing the BT-ID blend (Table S2, Supporting Information). In particular, diodes containing the BT-T2-ID blend exhibit the highest hole and electron mobilities among the blends of interest, at $1.7 \pm 0.1 \times 10^{-5}$ cm^2/V·s and $2.6 \pm 0.4 \times 10^{-4}$ cm^2/V·s, respectively. We thus speculate that the increase in device photocurrent with the extended isoindigo compounds stems from a combination of increased absorptivity as well as more efficient charge transport. With an increase in the number of octyl-thiophene units, we observe an increase in the V_{oc} from 0.84 V for devices containing the BT-T-ID blend to ca. 0.90 V for devices containing BT-T2-ID and BT-T3-ID blends, despite the observation that BT-T2-ID and BT-T3-ID have shallower HOMO energy levels compared to BT-T-ID. That the V_{oc} does not trend with the placement of the HOMO energy level of the neat constituents is not surprising because measurements of HOMO energy levels of the neat constituents do not account for interfacial dipoles and vacuum level misalignment that may be present in the bulk-heterojunction blends.[39] Importantly, differences in the solid-state morphology have also been reported to affect the V_{oc}.[40]

We carried out GIXD experiments to elucidate the structure of the photoactive layers; these GIXD images are provided in Figure S15 (Supporting Information). In Figure 5, we have extracted the azimuthally integrated intensity traces from the GIXD patterns. Comparing the X-ray diffraction traces across the as-cast blends, we observe that the primary peak in the diffraction trace of the blend containing BT-ID is substantially weaker than that of the primary peaks in the diffraction traces of the other blends. This observation suggests that blends containing extended isoindigo derivatives are more crystalline than those containing BT-ID. The GIXD images (Figure S15, Supporting Information) of all the blends show the same two meridional reflections as those in the GIXD images of the corresponding neat as-cast constituents, as well as an amorphous halo at 1.4−1.5 Å^{-1} corresponding to the presence of $PC_{71}BM$ or $PC_{61}BM$.[41,42] The incorporation of $PC_{71}BM$ and $PC_{61}BM$ does not appear to alter the placement of the primary reflection in the GIXD images of these isoindigo blends, suggesting that the isoindigo derivatives adopt structures in the photoactive layers that are similar to those in the as-cast constituent films.

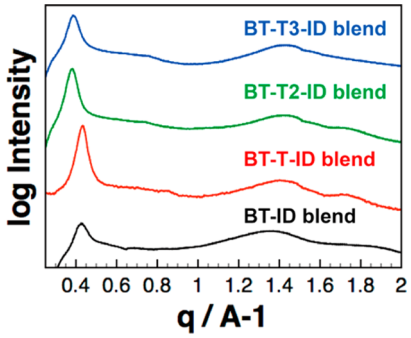

Figure 5. Azimuthally integrated intensity from the GIXD patterns of as-cast blended films.

While it is not immediately clear from the solid-state morphological characterization why BT-T2-ID should be the compound that yields the best devices among the isoindigo compounds studied, we note several remarkable distinctions with the compound. First, the absorption spectrum of the annealed BT-T2-ID film is red-shifted compared to BT-ID and BT-T-ID. Second, it also appears to be the most crystalline and ordered. Our characterization also indicates a very different molecular packing motif in BT-T2-ID compared to the other compounds. That BT-T2-ID outperforms the other compounds in photovoltaic devices is consistent with the observation made recently by Ma and co-workers with isoindigo polymers.[32] Devices comprising an isoindigo polymer having a bithiophene substitution similarly outperforms devices containing other polymers in the series having one and three thiophene units. In that study, the authors also attribute the high J_{sc} of devices containing the isoindigo polymer with the bithiophene unit to a higher absorptivity and an optimized morphology in the active layer.

AFM experiments were carried out to reveal the surface morphology of the as-cast blends, the images of which are shown in Figure 6. We observe large elongated structures and plate-like structures in the BT-ID and BT-T-ID blends, respectively. The surfaces of these blends are also rough, with an RMS roughness of 2.0 nm for blends containing BT-ID and 1.1 nm for blends containing BT-T-ID. On the contrary, we

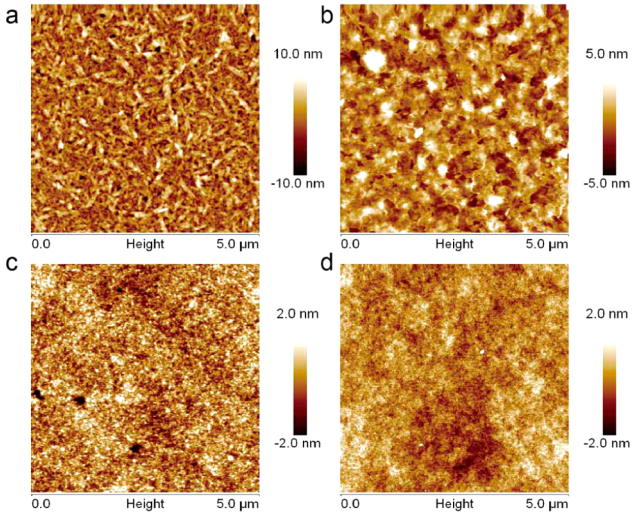

Figure 6. AFM images of as-cast blended films in the optimized devices comprising (a) BT-ID and $PC_{71}BM$; (b) BT-T-ID and $PC_{61}BM$; (c) BT-T2-ID and $PC_{61}BM$; and (d) BT-T3-ID and $PC_{61}BM$.

dx.doi.org/10.1021/cm503312c | Chem. Mater. 2014, 26, 6570−6577

observe much smaller domain sizes in blends containing BT-T2-ID and BT-T3-ID, with an RMS roughness of 0.5 and 0.4 nm, respectively. The smaller domain size and smoother surface in the blends of BT-T2-ID and BT-T3-ID suggest a higher extent of donor−acceptor interfaces and imply the opportunity for more efficient exciton dissociation and could thus be responsible for the improved performance over devices comprising BT-ID and BT-T-ID.

3.3. Photovoltaic Properties and Morphological Characteristics of the Annealed Devices. Devices containing the extended isoindigo derivatives were also subjected to thermal annealing. After thermal annealing at 70 °C, devices containing BT-T2-ID exhibit reduced V_{oc} (0.83 V) and J_{sc} (5.3 mA/cm^2), although the FF increased to 50%, resulting in a net PCE of 2.2% compared to 3.4% in the as-cast devices. Although they exhibit a lower average PCE after thermal annealing, devices containing annealed BT-T2-ID blends still out-perform devices containing other compounds studied here after thermal treatment. Devices containing the other isoindigo compounds also show a similar decrease in PCE after thermal annealing. Interestingly, in all cases, we observe an increase in FF with thermal annealing, although this increase comes at the expense of the J_{sc}. Because both the hole and electron mobilities increase with annealing (Table S2, Supporting Information), we surmise that charge transport cannot be the bottleneck responsible for the decreased photocurrents.

Complementary AFM images shown in Figure S16 (Supporting Information) reveal that the surface morphologies of BT-ID, BT-T-ID, BT-T2-ID, and BT-T3-ID blends have coarsened with thermal annealing, with higher RMS roughness of 5.3, 5.3, 1.3, and 0.5 nm, respectively, compared to their as-cast blends. This increase in the domain size could lead to a decrease in the donor−acceptor interfacial area that is available for charge separation.

4. CONCLUSIONS

The simple incorporation of oligothiophenes to extend backbone conjugation need not result in incremental changes in photophysical properties or solid-state structure development of molecular semiconductors. While the introduction of octyl-thiophene units between the isoindigo core and benzothiophene terminal groups has afforded us derivatives with smaller optical bandgaps, increased absorptivity, and enhanced ordering in the solid state, the improvements in properties are far from monotonic. In the series of extended isoindigo derivatives examined, BT-T2-ID appears to be unique in its photophysical property and solid-state organization; its incorporation in bulk-heterojunction solar cells resulted in the highest PCE among devices comprising isoindigo molecular semiconductors without additives.

Our studies thus point to the rich—and, in many ways, unexpected—solid-state structure development afforded by the incorporation of octyl-thiophene units to the isoindigo parent compound of BT-ID and highlight the incorporation of simple alkyl-substituted oligothiophenes as a possible tuning knob for dramatically altering the solid-state structure in molecular semiconductors.

■ ASSOCIATED CONTENT

Supporting Information

Details of synthetic procedures, GIXD images of as-cast neat films, as-cast and annealed blended films, UV−vis absorption spectra in $CHCl_3$ solutions and in as-cast blended films, and theoretical calculation data. This material is available free of charge via the Internet at http://pubs.acs.org.

■ AUTHOR INFORMATION

Corresponding Author

*Tel: +1 609-258-9091. E-mail: lloo@princeton.edu.

Notes

The authors declare no competing financial interest.

■ ACKNOWLEDGMENTS

This work was supported by ONR's Photovoltaic Program (N00014-11-10328), the SOLAR Initiative at the NSF (DMR-10135217), and an NSF-sponsored MRSEC through the Princeton Center for Complex Materials (Grant DMR-0819860), which also provided access to the PRISM Imaging and Analysis Center. GIXD experiments were conducted at CHESS, which is supported by NSF and NIH/NIGMS under award DMR-0936384. Y.R. thanks PCCM-MRSEC for a postdoctoral fellowship. A.K.H. is supported on an NSF graduate research fellowship. A.M.H is supported on an NDSEG graduate fellowship.

■ REFERENCES

(1) Mishra, A.; Bäuerle, P. *Angew. Chem., Int. Ed.* **2012**, *51*, 2020−2067.
(2) Henson, Z. B.; Müllen, K.; Bazan, G. C. *Nat. Chem.* **2012**, *4*, 699−704.
(3) Coughlin, J. E.; Henson, Z. B.; Welch, G. C.; Bazan, G. C. *Acc. Chem. Res.* **2014**, *47*, 257−270.
(4) Chen, Y.; Wan, X.; Long, G. *Acc. Chem. Res.* **2013**, *46*, 2645−2655.
(5) Lin, Y.; Li, Y.; Zhan, X. *Chem. Soc. Rev.* **2012**, *41*, 4245−4272.
(6) Beaujuge, P. M.; Fréchet, J. M. J. *J. Am. Chem. Soc.* **2011**, *133*, 20009−20029.
(7) Mei, J.; Graham, K. R.; Stalder, R.; Reynolds, J. R. *Org. Lett.* **2010**, *12*, 660−663.
(8) Graham, K. R.; Mei, J.; Stalder, R.; Shim, J. W.; Cheun, H.; Steffy, F.; So, F.; Kippelen, B.; Reynolds, J. R. *ACS Appl. Mater. Interfaces* **2011**, *3*, 1210−1215.
(9) Estrada, L. A.; Liu, D. Y.; Salazar, D. H.; Dyer, A. L.; Reynolds, J. R. *Macromolecules* **2012**, *45*, 8211−8220.
(10) Estrada, L. A.; Stalder, R.; Abbound, K. A.; Risko, C.; Brédas, J.-L.; Reynolds, J. R. *Macromolecules* **2013**, *46*, 8832−8844.
(11) Wang, E.; Mammo, W.; Andersson, M. R. *Adv. Mater.* **2014**, *26*, 1801−1826.
(12) Stalder, M. R.; Mei, J.; Graham, K. R.; Estrada, L. A.; Reynolds, J. R. *Chem. Mater.* **2014**, *26*, 664−678.
(13) Deng, Y.; Liu, J.; Wang, J.; Liu, L.; Li, W.; Tian, H.; Zhang, X.; Xie, Z.; Geng, Y.; Wang, F. *Adv. Mater.* **2014**, *26*, 471−476.
(14) Yassin, A.; Leriche, P.; Allain, M.; Roncali, J. *New J. Chem.* **2013**, *37*, 502−507.
(15) Liu, Q.; Du, Z.; Chen, W.; Sun, L.; Chen, Y.; Sun, M.; Yang, R. *Synth. Met.* **2013**, *178*, 38−43.
(16) Wang, T.; Chen, Y.; Bao, X.; Du, Z.; Guo, J.; Wang, N.; Sun, M.; Yang, R. *Dyes Pigm.* **2013**, *98*, 11−16.
(17) Yang, M.; Chen, X.; Zou, Y.; Pan, C.; Liu, B.; Zhong, H. *J. Mater. Sci.* **2013**, *48*, 1014−1020.
(18) Elsawy, W.; Lee, C.-L.; Cho, S.; Oh, S.-H.; Moon, S.-H.; Elbarbary, A.; Lee, J.-S. *Phys. Chem. Chem. Phys.* **2013**, *15*, 15193−15203.
(19) Takacs, C. J.; Sun, Y.; Welch, G. C.; Perez, L. A.; Liu, X.; Wen, W.; Bazan, G. C.; Heeger, A. J. *J. Am. Chem. Soc.* **2012**, *134*, 16597−16606.
(20) Welch, G. C.; Bakus, R. C.; Teat, S. J.; Bazan, G. C. *J. Am. Chem. Soc.* **2013**, *135*, 2298−2305.

(21) Walker, B.; Tamayo, A.; Dang, X.-D.; Zalar, P.; Seo, J. H.; Garcia, A.; Tantiwiwat, M.; Nguyen, T.-Q. *Adv. Funct. Mater.* **2009**, *19*, 3063−3069.
(22) Shin, W.; Yakuda, T.; Watanabe, G.; Yang, Y. S.; Adachi, C. *Chem. Mater.* **2013**, *25*, 2549−2556.
(23) Kim, C.; Liu, J.; Lin, J.; Tamayo, A. B.; Walker, B.; Wu, G.; Nguyen, T.-Q. *Chem. Mater.* **2012**, *24*, 1699−1709.
(24) Ren, Y.; Hiszpanski, A. M.; Whittaker-Brooks, L.; Loo, Y.-L. *ACS Appl. Mater. Interfaces* **2014**, 14533−14542.
(25) Frisch, M. J.; Trucks, G. W.; Schlegel, H. B.; Scuseria, G. E.; Robb, M. A.; Cheeseman, J. R.; Montgomery, Jr., J. A.; Vreven, T.; Kudin, K. N.; Burant, J. C.; Millam, J. M.; Iyengar, S. S.; Tomasi, J.; Barone, V.; Mennucci, B.; Cossi, M.; Scalmani, G.; Rega, N.; Petersson, G. A.; Nakatsuji, H.; Hada, M.; Ehara, M.; Toyota, K.; Fukuda, R.; Hasegawa, J.; Ishida, M.; Nakajima, T.; Honda, Y.; Kitao, O.; Nakai, H.; Klene, M.; Li, X.; Knox, J. E.; Hratchian, H. P.; Cross, J. B.; Bakken, V.; Adamo, C.; Jaramillo, J.; Gomperts, R.; Stratmann, R. E.; Yazyev, O.; Austin, A. J.; Cammi, R.; Pomelli, C.; Ochterski, J. W.; Ayala, P. Y.; Morokuma, K.; Voth, G. A.; Salvador, P.; Dannenberg, J. J.; Zakrzewski, V. G.; Dapprich, S.; Daniels, A. D.; Strain, M. C.; Farkas, O.; Malick, D. K.; Rabuck, A. D.; Raghavachari, K.; Foresman, J. B.; Ortiz, J. V.; Cui, Q.; Baboul, A. G.; Clifford, S.; Cioslowski, J.; Stefanov, B. B.; Liu, G.; Liashenko, A.; Piskorz, P.; Komaromi, I.; Martin, R. L.; Fox, D. J.; Keith, T.; Al-Laham, M. A.; Peng, C. Y.; Nanayakkara, A.; Challacombe, M.; Gill, P. M. W.; Johnson, B.; Chen, W.; Wong, M. W.; Gonzalez, C.; Pople, J. A. Gaussian 03, Revision E. 01, Gaussian Inc.: Wallingford, CT, 2007.
(26) Hiszpanski, A. M.; Lee, S. S.; Wang, H.; Woll, A. R.; Nuckolls, C.; Loo, Y.-L. *ACS Nano* **2013**, *7*, 294−300.
(27) Cai, T.; Zhou, Y.; Wang, E.; Hellström, S.; Zhang, F.; Xu, S.; Inganäs, O.; Andersson, M. R. *Sol. Energy Mater. Sol. Cells* **2010**, *94*, 1275−1281.
(28) Lakowicz, J. R. *Principles of Fluorescence Spectroscopy*, 3rd ed.; Springer: New York, 2006.
(29) Valeur, B. *Molecular Fluorescence, Principles and Applications*; Wiley-VCH: Weinheim, 2002.
(30) To reduce computation time, we replaced the ethylhexyl and octyl side chains with a methyl substituent for these calculations. These compounds are labeled BT-T-ID′, BT-T2-ID′, and BT-T3-ID′ in Table S1 in the Supporting Information.
(31) Spano, F. C.; Silva, C. *Annu. Rev. Phys. Chem.* **2014**, *65*, 477−500.
(32) Ma, Z.; Dang, D.; Tang, Z.; Gedefaw, D.; Bergqvist, J.; Zhu, W.; Mammo, W.; Andersson, M. R.; Inganäs, O.; Zhang, F.; Wang, E. *Adv. Energy. Mater.* **2014**, DOI: 10.1002/aenm.201301455.
(33) Hiszpanski, A. M.; Loo, Y.-L. *Energy Environ. Sci.* **2014**, *7*, 592−608.
(34) Hailey, A. K.; Hiszpanski, A. M.; Smilgies, D.-M.; Loo, Y.-L. *J. Appl. Crystallogr.* **2014**, DOI: 10.1107/S1600576714022006.
(35) Ma, Z.; Sun, W.; Himmelberger, S.; Vandewal, K.; Tang, Z.; Bergqvist, J.; Salleo, A.; Andreasen, J. W.; Inganäs, O.; Andersson, M. R.; Müller, C.; Zhang, F.; Wang, E. *Energy Environ. Sci.* **2014**, *7*, 361−369.
(36) Lei, T.; Dou, J.-H.; Pei, J. *Adv. Funct. Mater.* **2009**, *19*, 6457−6461.
(37) Chen, M. S.; Niskala, J. R.; Unruh, D. A.; Chu, C. K.; Lee, O. P.; Fréchet, J. M. J. *Chem. Mater.* **2013**, *25*, 4088−4096.
(38) Nagamatsu, S.; Kaneto, K.; Azumi, R.; Matsumoto, M.; Yoshida, Y.; Yase, K. *J. Phys. Chem. B* **2005**, *109*, 9374−9378.
(39) Guan, Z.-L.; Kim, J. B.; Wang, H.; Jaye, C.; Fisher, D. A.; Loo, Y.-L.; Kahn, A. *Org. Electron.* **2010**, *11*, 1779−1785.
(40) Qi, B.; Wang, J. *J. Mater. Chem.* **2012**, *22*, 24315−24325.
(41) Kang, S. J.; Ahn, S.; Kim, J. B.; Schenck, C.; Hiszpanski, O. S.; Schiros, T.; Loo, Y.-L.; Nuckolls, C. *J. Am. Chem. Soc.* **2013**, *135*, 2207−2212.
(42) Gomez, E. D.; Barteau, K. P.; Wang, H.; Toney, M. F.; Loo, Y.-L. *Chem. Commun.* **2011**, *47*, 436−438.